Simple Clothoid Lane Change Trajectories for Automated Vehicles Incorporating Friction Constraints

Joseph Funke[1]
Dynamic Design Laboratory,
Department of Mechanical Engineering,
Stanford University,
Stanford, CA 94305
e-mail: jfunke@stanford.edu

J. Christian Gerdes
Dynamic Design Laboratory,
Department of Mechanical Engineering,
Stanford University,
Stanford, CA 94305
e-mail: gerdes@stanford.edu

This paper demonstrates that an autonomous vehicle can perform emergency lane changes up to the friction limits through real-time generation and evaluation of bi-elementary paths. Path curvature and friction determine the maximum possible speed along the path and, consequently, the feasibility of the path. This approach incorporates both steering inputs and changes in speed during the maneuver. As a result, varying path parameters and observing the maximum possible entry speed of resulting paths give insight about when and to what extent a vehicle should brake and turn during emergency lane change maneuvers. Tests on an autonomous vehicle validate this approach for lane changes near the limits of friction. [DOI: 10.1115/1.4032033]

1 Introduction

As autonomous vehicles enter public roads, they must be capable of not only normal driving but also maneuvers to avoid accidents. For highway driving, an emergency lane change represents a particularly useful collision avoidance maneuver, enabling the vehicle to respond quickly to a blockage or other situation in the lane ahead. Such lane changes are ultimately limited by the friction between the tires and the road. Friction imposes coupled limits on a vehicle's lateral and longitudinal acceleration, constraining the total magnitude to no more than the tires' force generation capability (Fig. 1). In an emergency situation, a vehicle should quickly calculate a lane change trajectory that respects these limits.

The first step toward generating a lane change trajectory is to identify a path through space that avoids the obstacle. A series of straights and constant radius arcs can generate minimum length paths [1], but the resulting discontinuous path curvatures require instantaneous steering changes impossible for an autonomous vehicle to track [2]. Various smooth path functions for lane changes have been considered including exponentials, sinusoids, splines, and polynomials [3–5]. Alternatively, clothoid path segments, defined by linearly varying curvature, can interpolate between straights and arcs to generate continuous curvature paths. Clothoids are incorporated in road designs [6] and used for autonomous vehicle path tracking near the handling limits [7,8]. While any continuous curvature path could suffice for these applications, clothoids offer a simple yet sufficient solution.

The second step toward generating a lane change trajectory is to define the speed at which the vehicle should drive along the path. Desired speed dictates vehicle acceleration, which should not exceed the acceleration limits imposed by friction. A number of approaches assume either constant speed during the maneuver or speed variation within conservative, independent lateral and longitudinal acceleration limits [3–5]. These assumptions can simplify trajectory generation and are also incorporated into trajectory generation for more general situations that extend beyond lane changes. Top finishers in the DARPA Urban Challenge [9,10] and more recent research into trajectory generation [11,12] offer examples of this. However, these assumptions prevent full use of the available friction, which may be needed in some scenarios to avoid a collision. Kritayakirana and Gerdes's research into autonomous vehicle control near the handling limits calculates desired speeds for clothoid-based paths such that the vehicle does not exceed these modeled friction limits [7]. Other approaches use optimization techniques such as calculus of variations [13], series of convex optimizations [14], or nonlinear model predictive control [15] to generate trajectories at these friction limits.

In a real emergency, a lane change trajectory must not only utilize friction within these limits but it must also be calculable in real-time. Otherwise, the vehicle could be too late responding to a threat. The computational overhead of the optimization techniques makes real-time implementation challenging [13–15]. Kritayakirana and Gerdes's approach relies on clothoid-based paths generated by an offline solver, because no closed-form solutions for spatial clothoid parameters exist [7,8]. However, Scheuer and Fraichard describe a subset of clothoid-based paths called bi-elementary paths for which closed-form expressions do exist [2], allowing this subset of paths to be calculable in real-time.

Bi-elementary paths are used in this work to quickly generate lane change paths. A speed profile calculation based on Kritayakirana and Gerdes's approach [7] then calculates velocities that do

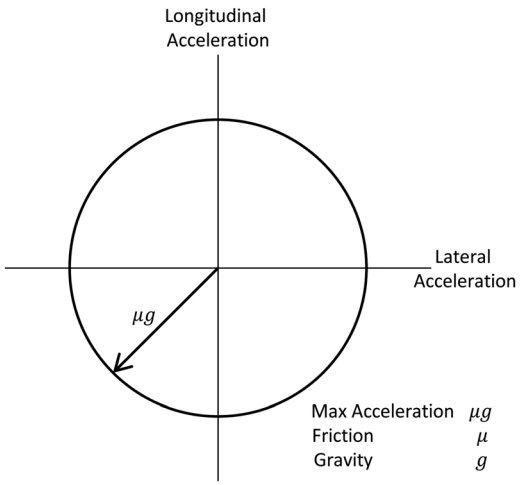

Fig. 1 Acceleration limits based on a friction circle model

[1]Corresponding author.

Contributed by the Dynamic Systems Division of ASME for publication in the Journal of Dynamic Systems, Measurement, and Control. Manuscript received July 1, 2013; final manuscript received November 15, 2015; published online December 11, 2015. Editor: Joseph Beaman.

not exceed modeled friction limits. An autonomous vehicle can generate and evaluate the resulting trajectories in real-time and drive them at these friction limits. Analyzing such trajectories also suggests relative roles of braking and steering to maximize the number of situations in which an emergency lane change can be completed. For example, pure braking followed by steering is undesirable in all but a few cases; however, steering while braking is advantageous, and the relative amount of steering and braking depends on the lane change.

This paper begins by introducing the generalized elementary and bi-elementary path, followed by a method of using the friction limit to determine the maximum speed a vehicle can track a given path. These tools are used to discuss trends arising from the variation of path parameters; these trends offer insight into the relative roles of braking and steering. The process is then demonstrated on an autonomous vehicle, verifying the method of trajectory generation on a real vehicle.

2 Lane Change Paths

A lane change maneuver transitions a vehicle from one straight lane into another. Lane changes can be defined by a longitudinal distance X along the road during which the lane change occurs and a lateral displacement Y, which is the width of a lane. A third parameter μ, the friction coefficient between the road surface and the vehicle's tires, defines the vehicle's acceleration limits. A vehicle's heading at the beginning and end of a lane change should both be equal to the heading of the lane, ψ_{lane}, so that the vehicle starts and concludes the maneuver driving in the direction of the lane. Given a lane change defined by X, Y, and μ, a path parametrized by γ, β, and λ can complete the lane change. Figure 2 depicts the lane change setup and a path. Table 1 defines the associated parameters.

Clothoid-based paths parametrized by γ, β, and λ can describe lane changes of arbitrary X, Y, and μ values. Because clothoids in general lack closed-form solutions, some applications, such as calculating racing lines, use iterative techniques to determine the necessary clothoid parameters [8]. However, a subset of clothoid-based paths called elementary and bi-elementary paths restrict paths to a subset with quickly calculable solutions, which is useful for real-time path generation. This section introduces clothoids and their relationship to straights and arcs, defines the generalized elementary path, and introduces the concept of bi-elementary paths.

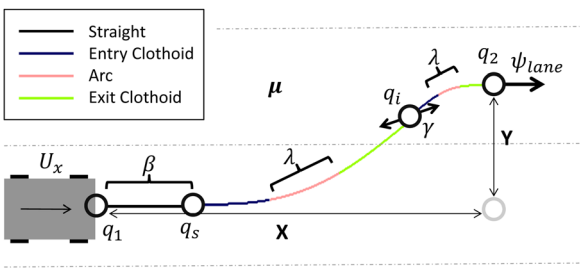

Fig. 2 Lane change and path parameters

Table 1 Parameters defining a lane change situation and a lane change path

Lane change parameters		
μ	Friction coefficient between road/tires	
X	Longitudinal distance of lane change	
Y	Lateral displacement of lane change	
Path parameters		
γ	Symmetric point fraction	(determines q_i)
β	Straight length fraction	(determines q_s)
λ	Arc length fraction	(determines L_{arc})

2.1 Path Primitives. All of the paths discussed here consist of three path primitives: straights, arcs, and clothoids. Each path segment is defined by curvature k as a function of distance s along the segment. A straight is a path segment with zero curvature, $k(s) = 0$. An arc has a constant nonzero curvature of $k(s) = 1/R$, where R is the radius of the arc. A clothoid is defined by a linearly varying curvature along its length, $k(s) = \sigma s$, where σ is the rate of change of curvature, or sharpness. For all of these primitives, the tangent direction along the path, or heading, and the positions along the path are given by

$$\psi(s) = \int_0^s k(z)dz + \psi_0 \tag{1}$$

$$x(s) = \int_0^s \cos\psi(z)dz + x_0 \tag{2}$$

$$y(s) = \int_0^s \sin\psi(z)dz + y_0 \tag{3}$$

where s is defined over the interval $[0, L_{\text{seg}}]$.

2.2 Generalized Elementary Path. Two clothoids of equal length and opposite sharpness comprise an elementary path [2]. The first clothoid, or "entry clothoid," begins with zero curvature, and the second, "exit clothoid," ends with zero curvature. In this work, the elementary path is generalized to include an arc between the entry and exit clothoids, giving an extra degree-of-freedom in path selection. The parameter λ defines the length of the arc as a fraction of the total length of the generalized elementary path

$$\lambda = \frac{L_{\text{arc}}}{L} \tag{4}$$

A curvature profile of

$$k(s) = \begin{cases} \sigma s & \forall s \in \left[0, L\dfrac{1-\lambda}{2}\right] \quad \text{Entry clothoid} \\ \sigma L\dfrac{1-\lambda}{2} & \forall s \in \left(L\dfrac{1-\lambda}{2}, L\dfrac{1+\lambda}{2}\right) \quad \text{Arc} \\ \sigma(L-s) & \forall s \in \left[L\dfrac{1+\lambda}{2}, L\right] \quad \text{Exit clothoid} \end{cases} \tag{5}$$

thus defines a generalized elementary path (see Fig. 3).

As shown in Eq. (5), a generalized elementary path is defined by arc length fraction λ, sharpness σ, and path length L. For any choice of λ, σ and L dictate the positions through which an

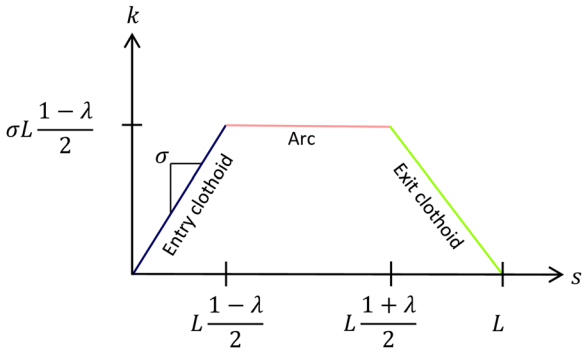

Fig. 3 Generalized elementary path curvature profile

elementary path passes. Substituting Eq. (5) into Eqs. (1)–(3) yields expressions for path position but, given a desired ending position, these expressions cannot be directly solved for σ and L. Another approach is taken instead.

To calculate σ and L, the notion of configurations is useful. A configuration q is comprised of a position (x, y) and a heading ψ. Configuration $q_1 = (x_1, y_1, \psi_1)$ is the initial position and heading at the beginning of a lane change, and $q_2 = (x_2, y_2, \psi_2)$ is the position and heading at the end of a lane change. A generalized elementary path can begin at q_1 and end at any q_2 with a predefined heading and a forward facing position, i.e., a position (x_2, y_2) for which the angle between ψ_1 and a line from (x_1, y_1) to (x_2, y_2) is less than $\pi/2$.

The heading of q_2 is specified by a key property of elementary paths. By definition, the curvature profile of these paths is a symmetric function, so only symmetric configurations can be joined by a single path. A symmetric configuration is one in which

$$\alpha = \psi_2 - \psi_1 = 2\tan^{-1}\left(\frac{y_2 - y_1}{x_2 - x_1}\right) \tag{6}$$

holds true, where $\alpha \in (-\pi, \pi)$ is the deflection, or change in heading along the path. Practically, this means any forward facing position can be reached via an elementary path with an end heading specified by Eq. (6). The intuition here is that because the path has a symmetric curvature function, the headings at the start and end of the path must have the same offset angle from the line connecting the two positions (see Fig. 4).

The goal is to find the σ and L that connect two symmetric configurations. Given two configurations, the Euclidean distance between them is

$$d = \sqrt{(x_2 - x_1)^2 + (y_2 - y_1)^2} \tag{7}$$

The change in heading α along a generalized elementary path is given by

$$\alpha = \psi_2 - \psi_1 = \int_0^L k(z)dz = \frac{\sigma L^2}{4}(1 - \lambda^2) \tag{8}$$

from substituting Eq. (5) into Eq. (1). The "size" $D(\alpha, \lambda)$ is the ratio of the Euclidean distance d and the length L of the path connecting them, $D(\alpha, \lambda) = d/L$, where d and L are shown in Fig. 4. Rearranging Eq. (8) and the definition of D yields the desired equations for L and σ

$$L = \frac{d}{D(\alpha, \lambda)} \tag{9}$$

$$\sigma = \frac{4\alpha}{L^2(1 - \lambda^2)} \tag{10}$$

where d is given by Eq. (7) and α is given by Eq. (6) for a pair of symmetric configurations.

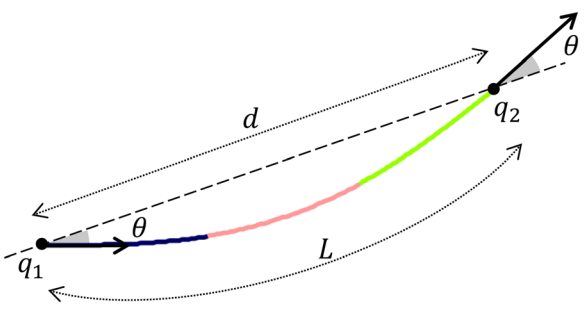

Fig. 4 Symmetry of generalized elementary path

$D(\alpha, \lambda)$ can be found from the geometry of a symmetric path given α and λ. Following the general approach to derive D provided by Kanayama and Hartman [16], $D(\alpha, \lambda)$ for a generalized elementary path is

$$D(\alpha, \lambda) = 2\int_0^{0.5} \cos\psi(z)dz \tag{11}$$

where $\psi(z)$ is given by

$$\psi(z) = \begin{cases} \dfrac{2\alpha}{1+\lambda}z & \forall z \in \left[0, \dfrac{\lambda}{2}\right] \quad \text{Arc} \\ \dfrac{2\alpha}{1-\lambda^2}\left(-z^2 + z - \dfrac{\lambda^2}{4}\right) & \forall z \in \left(\dfrac{\lambda}{2}, \dfrac{1}{2}\right] \quad \text{Exit clothoid} \end{cases} \tag{12}$$

$D(\alpha, \lambda)$ can be negative, resulting in a negative (and thus infeasible) length in Eq. (9), but this does not occur for forward facing points. More detail on this limitation can be found in Scheuer and Fraichard's paper [2].

2.3 Bi-Elementary Path. An elementary path can join two symmetric configurations, but configurations defining the start and end of a lane change are not symmetric. However, a bi-elementary path can connect two nonsymmetric configurations to generate a lane change path. Given two configurations, an intermediate configuration called the symmetric configuration, q_i, exists and is symmetric with both q_1 and q_2. An elementary path can connect q_1 to q_i and a second elementary path can connect q_i to q_2, where the heading ψ_i is constrained by Eq. (6). The resulting two-elementary path segment is a bi-elementary path.

Assuming the starting and ending headings are equal, as is the case for a lane change, the locus of symmetric configurations for a given q_1 and q_2 lies on the line between q_1 and q_2

$$y_i = \frac{y_2 - y_1}{x_2 - x_1}x_i + y_1 \tag{13}$$

A proof of Eq. (13) is available in Ref. [16]. Different symmetric configurations result in different bi-elementary paths connecting q_1 and q_2. Configurations on the line not between q_1 and q_2 result in impractical solutions, so the symmetric configuration position is restricted to within q_1 and q_2. The location of q_i is parametrized by γ, where γ defines the fraction of the distance between q_1 and q_2

$$\gamma = \frac{\text{Distance of } q_i \text{ from } q_1}{\text{Distance of } q_2 \text{ from } q_1} = \frac{\sqrt{(x_i - x_1)^2 + (y_i - y_1)^2}}{\sqrt{(x_2 - x_1)^2 + (y_2 - y_1)^2}} \tag{14}$$

As γ approaches zero, q_i approaches q_1; as γ approaches one, q_i approaches q_2.

2.4 Adding a Straight. A bi-elementary path connects two configurations. So far the configurations have been q_1 at the start of the lane change and q_2 at the end of the lane change, with q_i in between. An additional configuration q_s can be added along the line extending from q_1 in the direction of the lane. q_1 and q_s can be connected by a straight, and q_s and q_2 are connected by a bi-elementary path as before. β parametrizes the length of the straight as a fraction of the longitudinal distance between configurations

$$\beta = \frac{L_{\text{straight}}}{X} = \frac{(x_s - x_1)\cos\psi_1 + (y_s - y_1)\sin\psi_1}{(x_2 - x_1)\cos\psi_1 + (y_2 - y_1)\sin\psi_1} \tag{15}$$

The resulting path stays in the current lane for a distance specified by β before initiating the lane change.

The symmetric point fraction γ, straight length fraction β, and arc length fraction λ represent the set of variable path parameters and are depicted in Fig. 2.

3 Speed Profile of a Path

Bi-elementary paths can describe lane changes; however, these paths cannot be driven at arbitrarily high speeds. Therefore, it becomes necessary to determine the maximum speed that a vehicle can drive along a path. Path curvature and the available friction μ determine this maximum speed at each point along the path, defining the path's speed profile. A speed profile thus provides an upper speed bound; any speeds below the speed profile are within the friction limits. The exit speed is the final value of a speed profile, corresponding to the maximum possible vehicle speed at the end of the path. The entry speed is the first value of the speed profile, representing the maximum possible vehicle speed at the beginning of the path.

The entry speed of a path can be used as a metric of path feasibility. If a vehicle's current speed is less than a proposed path's entry speed, then the vehicle can follow that path while remaining within the friction limits. Otherwise, the vehicle is traveling too fast to track the path, which is deemed infeasible. Entry speeds, and thus speed profiles, determine path feasibility.

3.1 Derivation. A speed profile is based on a point mass representation of a vehicle with friction limits. The friction circle, as shown in Fig. 1, is a common representation of this limitation

$$\sqrt{a_x^2 + a_y^2} \leq \mu g \tag{16}$$

where a_x and a_y are the longitudinal and lateral accelerations of the vehicle, and g is gravitational acceleration. Driving at the limits equates to accelerating or decelerating in ways that utilize all available friction, making Eq. (16) an equality. Assuming a point mass model, the lateral acceleration a_y of a vehicle tracking a path with curvature k is

$$a_y \approx \frac{U_x^2}{R} = U_x^2 k \tag{17}$$

From Eqs. (16) and (17), the maximum speed at a point along the path with a given curvature k is

$$U_x = \sqrt{\frac{a_y}{k}} = \sqrt{\frac{\mu g}{k}} \tag{18}$$

The speed profile calculation starts with the local maximum curvature points along a path. Two such points exist for bi-elementary paths (k_1 and k_2 in Fig. 5). U_x at these points are given by Eq. (18). Substituting Eq. (17) into Eq. (16) yields

$$a_x(s_n) = \sqrt{(\mu g)^2 - (U_x(s_n)^2 k(s_n))^2} \tag{19}$$

which determines the maximum possible longitudinal acceleration at each successive distance s_n along the path. Speeds at points along the path before and after a local maximum curvature point are found by Euler integration where a_x is given by Eq. (19) and time t is given by

$$t(s_n) = \frac{-U_x(s_n) + \sqrt{U_x(s_n)^2 + 2a_x(s_n)(s_{n+1} - s_n)}}{a_x(s_n)} \tag{20}$$

assuming constant acceleration between points and positive time values. The resulting difference equation is

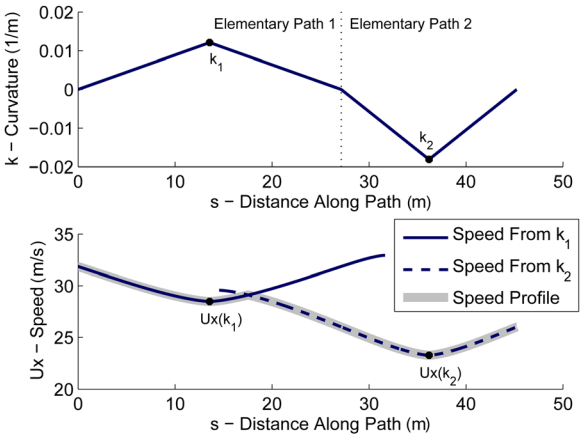

Fig. 5 Determining a speed profile for a path

$$\begin{aligned} U_x(s_{n+1}) &= U_x(s_n) + t(s_n)a_x(s_n) \\ &= \sqrt{U_x(s_n)^2 + 2a_x(s_n)(s_{n+1} - s_n)} \end{aligned} \tag{21}$$

Integration continues until either the end of the path is reached or $(U_x(s_n)^2 k(s_n))^2 > (\mu g)^2$ and Eq. (19) becomes imaginary (indicating the speed is too high for the given curvature). Each local maximum curvature point thus results in a separate speed profile, two in the case of a bi-elementary path. The actual speed must be low enough to satisfy all of these constraining speeds, so the minimum speed of all profiles at each point along the path is taken as the final speed profile. An example is shown in Fig. 5 where two speed profiles are calculated and the minimum of the two yields the final speed profile.

3.2 Other Effects. The speed profile derivation uses a point mass model that ignores the vehicle's moment of inertia and assumes motion in a plane. A point mass model does not differentiate between a front and rear axle, which will have different and variable friction limits throughout a lane change maneuver. Longitudinal weight transfer shifts the normal load between the front and rear axle, affecting available friction at each axle. Road bank, or angle of slant, shifts normal loads and requires some lateral acceleration to prevent lateral sliding. Road grade, or angle of elevation, shifts normal loads and offsets available longitudinal acceleration. Longitudinal weight transfer, bank, and grade can be added to the speed profile calculation, modifying Eq. (16) and thus Eq. (19) to provide a more accurate speed profile specific to a particular vehicle and road layout. Adding these effects is fully described by Kritayakirana [17]. Speed profile calculation including these effects has been successfully used for autonomous vehicle control near the handling limits [7,17].

Load transfer, bank, and grade are included in the speed profile calculation when running lane change experiments on an autonomous vehicle. These effects are not considered when evaluating general trends in Sec. 4 because they do not alter the intuition gained.

4 Trends Observed in Bi-Elementary Lane Change Paths

A family of bi-elementary paths can complete a given lane change, and each path will have its own speed profile and associated entry and exit speed. Exit speeds are discussed because they bound the maximum possible speed at the end of a maneuver, which may be useful to know in situations such as switching into a lane with faster traffic. More importantly, a higher entry speed increases the range of vehicle speeds for which the lane change maneuver is feasible, increasing the number of situations in which

a vehicle could switch out of an unsafe lane. For this reason, path parameters that generate the path with the greatest entry speed are sought. Finding these path parameters can also extend from a specific lane change to consider all lane changes. Varying only the ratio of X to Y encapsulates trends for all lane changes defined by X, Y, and μ.

This section first introduces the lane change ratio X/Y and explains its parametrization of all lane changes. Then, path parameters γ, β, and λ are each determined to maximize entry speed. Each parameter modifies the path in a structured manner that maps to steering and braking commands. The section then concludes with trends from all the path parameters. Note that the following analysis focuses on trajectory selection assuming immediate tire force generation, so effects that limit force generation such as tire relaxation and brake delay are not considered.

4.1 The Lane Change Ratio. A lane change is defined by X, Y, and μ as shown in Fig. 2, but only the ratio of X to Y changes trends in the speed profiles as path variables are varied. Scaling μ by c_1 simply scales the path's speed profile by $\sqrt{c_1}$, which is evident from Eqs. (18) and (21). Scaling both X and Y by a constant c_2 adjusts the path length and scales the speed profile by $\sqrt{c_2}$. This can be seen by examining the equations for bi-elementary paths and speed profile calculation. The resulting entry speeds in both cases are scaled by $\sqrt{c_1}$ and $\sqrt{c_2}$.

Unlike these scalings, the lane change ratio X/Y nontrivially affects the speed profile and entry speed. A lane change defined by a lower ratio of 10 (37 m of distance assuming a normal road width of 3.7 m) is fundamentally different from a lane change with a higher ratio of 25 ($\approx$ 93 m of distance to change lanes) and requires a different kind of path. Due to the scaling properties, a path parameter argument maximizing entry speed for one lane change ratio also maximizes entry speeds for all lane changes with that ratio. As a result, the value of a path parameter that maximizes entry speeds over all possible lane changes can be evaluated by comparing maximal parameter values over lane changes defined by a range of lane change ratios.

4.2 Early Versus Late Steering: Varying γ

4.2.1 Fixed Lane Change Ratio of 45/3.7. Varying the symmetric point fraction γ changes the location of q_i along the line between q_1 and q_2, biasing path curvature toward the beginning or end of the lane change. Results from varying γ are shown in Fig. 6 for a lane change defined by $X = 45$ m, $Y = 3.7$ m, and $\mu = 1$. The first plot shows the resulting paths. As γ increases, q_i shifts toward q_2 and lateral displacement occurs later along the path. The curvature profiles shown in the second plot explain this shift. When $\gamma < 0.5$, the first elementary path (from q_1 to q_i) has greater sharpness and a greater maximum curvature, which biases lateral movement to this first elementary path. When $\gamma > 0.5$, the second elementary path (from q_i to q_2) has greater sharpness and curvature, biasing lateral movement to the second elementary path. When $\gamma = 0.5$, the first and second elementary paths have equal length and sharpness of equal but opposite magnitude.

High path curvature requires large steering inputs and leaves little friction for longitudinal inputs. As a result, a low γ path requires large steering inputs early in the maneuver, allowing acceleration only after most of the lane change is completed. A high γ path, however, requires large steering inputs later in the maneuver, allowing braking to occur early in the maneuver. The speed profiles in the third plot of Fig. 6 illustrate the resulting tradeoffs in the speed profile, with a low γ path offering high exit speeds and a high γ path offering high entry speeds.

The symmetric point fraction γ determines where the path curvature and thus steering and longitudinal inputs becomes large, trading off between entry speed, exit speed, and path location. Lower γ paths bias larger curvature magnitudes to the first elementary path. Larger initial curvature decreases entry speed but provides an earlier shift into the new lane. Smaller curvatures of

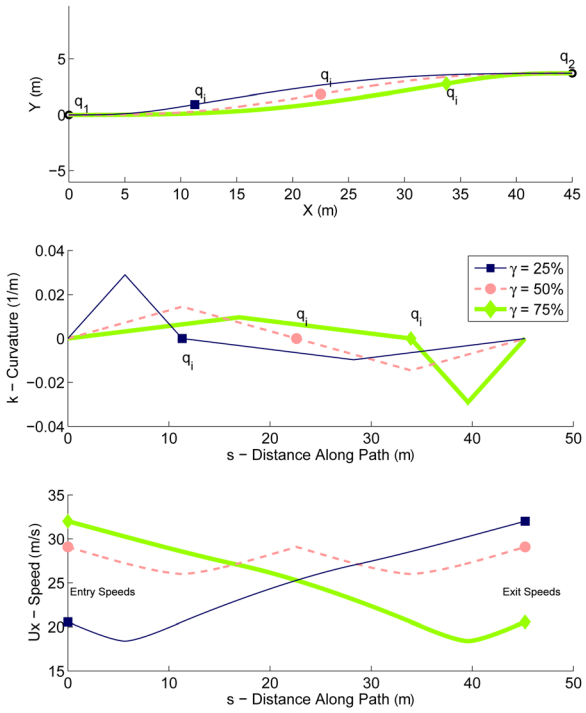

Fig. 6 Varying γ for a lane change path

the second elementary path increase the exit speed. Higher γ paths bias larger curvature magnitudes to the second elementary path. The resulting paths have increased entry speeds but decreased exit speeds and shift into the new lane later. $\gamma = 0.5$ yields the minimum curvature path. If braking were not possible and a constant speed were held through the lane change, then this would be the path with the highest speed, as defined in Eq. (18). With the ability to brake, the minimum curvature path no longer becomes the solution with the highest entry speed.

4.2.2 Varied Lane Change Ratio. The results so far consider one lane change ratio, and the value of γ that maximizes entry speed is a function of this ratio. As the ratio decreases, the value of γ maximizing entry speed increases, further biasing the path and suggesting later steering. Figure 7 demonstrates this trend as the ratio varies (Y held constant at 3.7 m and X varied). The actual speed changes significantly with X, so the values are normalized to the maximum entry speed for each X; otherwise, the relative effect of γ is lost in the absolute change in entry speed as X varies. The black line highlights the value of γ achieving the maximum

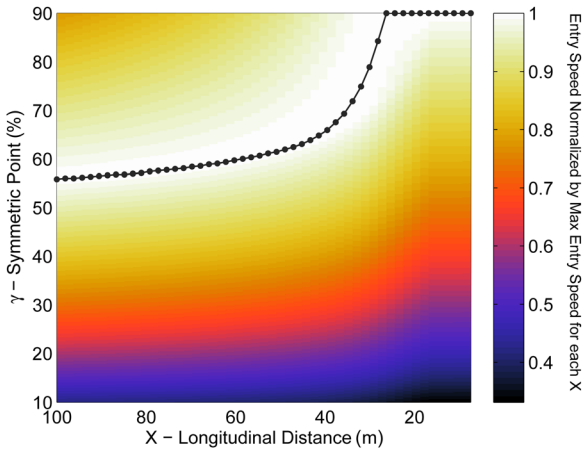

Fig. 7 γ maximizing entry speed as X varies

entry speed. For large X (large ratio), less biased paths with $\gamma \approx 0.5$ yield the highest entry speeds. However, as the longitudinal distance X decreases, γ shifts higher. This shift occurs because the resulting paths allow additional braking distance to slow down for the larger curvatures. The maximum entry speed path corresponds to the γ producing a curvature profile conducive to braking throughout the maneuver. This occurs when the speed profile generated from the second maximum curvature point k_2 in Fig. 5 has a speed at k_1 equal to $U_x(k_1)$. These results suggest that simultaneously braking and steering increases the family of feasible paths, and the proportion of braking to steering along the lane change path depends on the lane change's horizontal distance.

4.2.3 Limitation. Vehicles have physical limitations not captured by the point mass model including underlying transient dynamics, turning limits, and steering rate limits. While $\gamma \to 1$ achieves maximum entry speed paths for low lane change ratios, the resulting second elementary paths have increasingly large sharpness and curvature. Vehicle limitations such as turning limits and steering rate limits will place upper bounds on practical limits of path curvature and sharpness. As a result, these limit cases of high γ cannot be realized on a real vehicle.

4.3 Straight Line Braking: Varying β

4.3.1 Fixed Lane Change Ratio of 30/3.7. Increasing the straight length fraction β increases the length of a straight before the bi-elementary path, increasing the distance during which all available friction is used entirely for braking (rather than steering). Figure 8 shows an example of a path with no straight and a path with half of the available longitudinal distance X set to be a straight. This is a special case where these two paths result in nearly the same entry speed. However, adding the straight decreases the exit speed.

4.3.2 Varied Lane Change Ratio. The value of β that maximizes entry speed also changes with the lane change ratio. The general trend as X changes is shown in Fig. 9, with symmetric point fraction $\gamma = 0.5$ and arc length fraction $\lambda = 0$. The black line in Fig. 9 represents the normalized maximum entry speed. The path that maximizes entry speed has either no straight or the

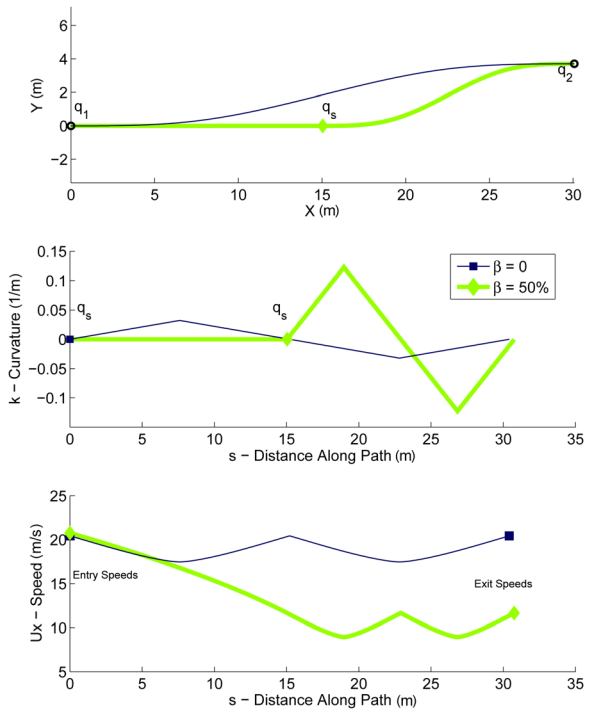

Fig. 8 Varying β for a lane change path

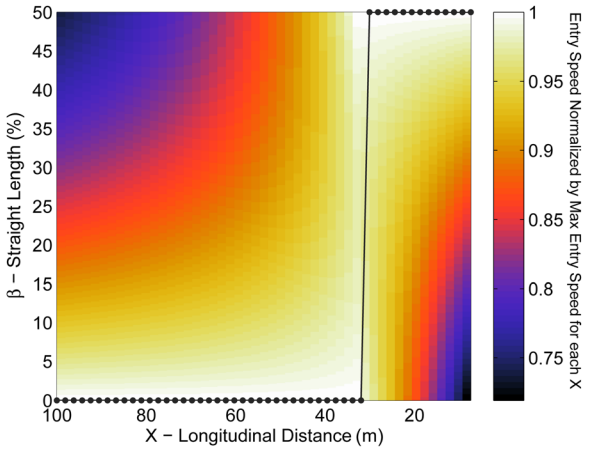

Fig. 9 β maximizing entry speed as X varies

maximum allowable straight; midlength straights never maximize entry speed. This suggests that a vehicle should either brake without turning for as long as possible or immediately turn and brake. Braking before turning maximizes entry speed when X is small, corresponding to a low lane change ratio or high lateral displacement. Braking before a large lateral displacement makes sense considering a vehicle approaching a normal turn. However, a lane change ratio exists above which straight line braking becomes undesirable because entry and exit speeds decrease. The lane change ratio when this switch occurs depends on both γ and λ. Besides maximizing entry speeds, varying β could be useful in certain situations, such as braking to let another car pass before completing the lane change.

4.3.3 Limitation. Adding a straight reduces the longitudinal distance for the bi-elementary path, substantially increasing the curvature and sharpness of the path. As with symmetric point fraction γ, curvature and sharpness limitations will bound the possible values of β. Nonzero β improves entry speed for small X where curvatures and sharpness are already large, so β will be severely limited by these bounds.

4.4 Faster Steering: Varying λ

4.4.1 Fixed Lane Change Ratio of 15/3.7. Increasing the length of the arcs in the path with λ decreases the maximum curvature along that path but increases the sharpness. Lower maximum curvature reduces the magnitude of steering required. However, greater sharpness corresponds to higher curvature rates and faster steering. The resulting paths, as shown in Fig. 10, allow higher speeds throughout the maneuver. These results suggest that greater sharpness and thus faster steering results in paths with higher entry and exit speeds.

4.4.2 Varied Lane Change Ratio. Increasing the arc length fraction λ increases the entry speed for all but the smallest values of X, as shown in Fig. 11. Unlike β, which maximizes entry speed with either the minimum or maximum value, nonextremal values of λ also maximize entry speed for a small range of X at low lane change ratios. Also, as shown by the scales of normalized entry speed in Figs. 7, 9, and 11, λ has less total effect on entry speed than γ or β.

4.4.3 Limitation. As $\lambda \to 1$, the entry and exit speeds increase, but the resulting path approaches two arcs with infinite sharpness and a discontinuous curvature profile. Such a discontinuity is impossible for a vehicle to track, requiring the wheels to instantaneously turn. Paths with $\lambda = 0$ and no arc have the lowest sharpness, which requires the slowest steering rates and are the easiest to track; however, these paths have the slowest speed

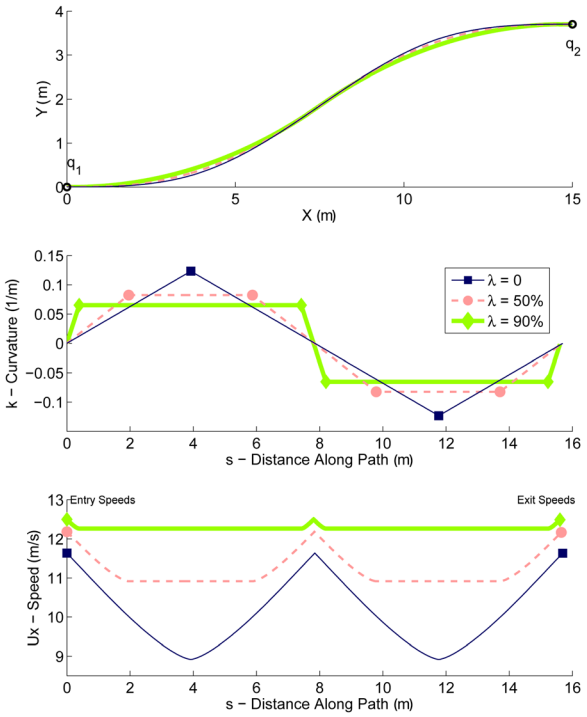

Fig. 10 Varying λ for a lane change path

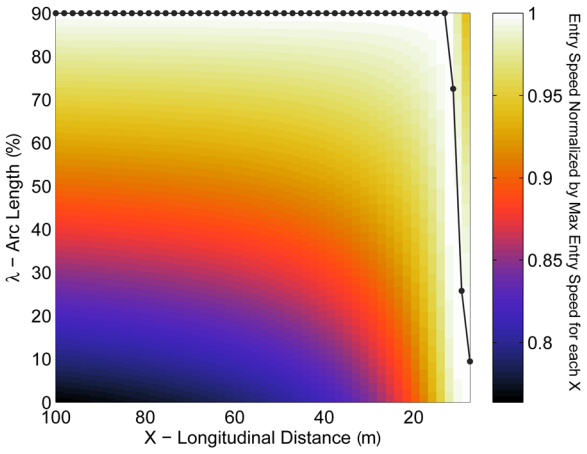

Fig. 11 λ maximizing entry speed as *X* varies

profiles. Thus, a tradeoff exists between the vehicle's steering effort and the path's speed profile.

Transient dynamics and steering controller design also become critical as λ increases, as either tracking performance or stability will degrade while attempting to track these paths. However, for the test vehicle used here and other vehicles using commercial electric power steering systems, the choice of λ is first limited by the maximum achievable steering rate of the vehicle.

4.5 Summary of Trends. The trends for each individually varied path parameter still hold when all three parameters are simultaneously changed. For lane changes with a high lane change ratio, highest entry speed paths are achieved with no straights ($\beta = 0$) and maximum length arcs ($\lambda \to 1$). The path starts nearly symmetric ($\gamma = 0.5$), and as the lane change ratio decreases (decreasing longitudinal distance assuming a fixed lane width), paths skew toward biasing lateral deviation to the second elementary path ($\gamma \to 1$). As paths skew, braking begins to dominate early in the maneuver followed by steering. For low ratio lane changes, adding straights and decreasing the length of arcs produce the maximum entry speed paths.

5 Experiments

Experiments confirm that these clothoid-based trajectories can be used for real-time lane change obstacle avoidance at the modeled friction limits.

5.1 Setup. These tests were conducted using the Audi TTS pictured in Fig. 12. This vehicle can operate autonomously near the limits of handling while tracking paths composed of straights, clothoids, and arcs [18]. A virtual obstacle, defined as a required lateral offset for the vehicle to achieve by a specified distance along the straight, appeared while driving and within 5 ms an on-board computer calculated a lane change path and provided it to the path tracking controller.

Based on the trends previously discussed, only the symmetric point fraction γ was varied to find a family of lane change paths. The arc length fraction λ remained at 0 to minimize sharpness, reducing the required steering rates to within the vehicle's steering ability. Lane change distances were large enough that $\beta = 0$ maximized entry speeds, so the straight length fraction β was set to 0. Rather than finding the maximum entry speed path, γ was varied to match the path's entry speed to the vehicle's current speed, plus an offset to account for delay in brake actuation. Path entry speed was reduced to the current vehicle speed because, as shown in Fig. 6, decreased γ enables higher exit speed and produces lateral movement earlier in the maneuver.

The resulting online algorithm set $\lambda = 0$, $\beta = 0$, and bisected to determine γ, detailed in Algorithm 1. At each bisection iteration, the algorithm generated the bi-elementary path, evaluated the speed profile, and selected the next γ guess based on the path's entry speed compared the vehicle's current speed. Bisection terminated after a fixed number of iterations to ensure consistent execution times, which remained below 5 ms using the on-board 1.8 GHz Pentium M computer.

Fig. 12 Autonomous Audi TTS

Algorithm 1 Bisecting the symmetric point fraction γ

γ_{min} = lower bound
γ_{max} = upper bound
for desired number of iterations **do**
  $\gamma_{guess} = 0.5(\gamma_{min} + \gamma_{max})$
  generate path with $\gamma = \gamma_{guess}$, $\lambda = 0$, $\beta = 0$
  calculate speed profile
  if current speed > path entry speed **then**
    $\gamma_{min} = \gamma_{guess}$
  else
    $\gamma_{max} = \gamma_{guess}$
  end if
end for
return trajectory defined by $\gamma = \gamma_{guess}$, $\lambda = 0$, $\beta = 0$

The resulting trajectories were designed to use all of the available friction between the road and tires. The vehicle had standard passenger car tires and operated on an asphalt surface. Friction was estimated from the maximum acceleration generated from a quasi-steady state ramp steer maneuver conducted prior to the tests. Other vehicle parameters are available in Ref. [17]. As previously mentioned, the speed profile calculation and friction circle were modified from Eq. (21) to account for weight transfer, bank, and grade.

5.2 Results. The vehicle cruised at speeds of 20 m/s, 25 m/s, and 30 m/s and detected the virtual obstacle at the point (0, 0) along the path. Figure 13 shows the lane change parameters ($X = 50$ m, $Y = 3.7$ m, and $\mu = 0.82$) and the resulting paths for the different speeds. The tracking error at the end of the lane change was within 12 cm in all cases. Figure 14 shows the speed profile and the actual vehicle speed for each lane change. The vehicle braked to track decelerating speeds well, which is important since speeds should not exceed the speed profile. The vehicle tracked accelerations less well due to engine lag and power limits common to any production vehicle; however, speeds erroring below the speed profile are acceptable and simply entail incomplete friction usage during acceleration. Figure 15 plots the friction circle, modified to incorporate weight transfer, along with the accelerations at the vehicle's center of gravity for each test.

While traveling at 20 m/s, the vehicle detected the obstacle and calculated a path with symmetric point fraction $\gamma = 0.27$, pictured in Fig. 13. This path biased larger curvatures to the first elementary path and moved the vehicle into the new lane earlier in the lane change. The vehicle quickly braked then accelerated through the rest of the maneuver, as shown in Fig. 14. The resulting vehicle accelerations tracked the friction circle in Fig. 15, at least within the acceleration limits of the engine. In the results presented here, the vehicle accelerated when possible during the lane change in an attempt to track the speed profile and remain near the friction limits. In practice, the vehicle only needs to remain within the friction limits, so vehicle speeds can remain below the speed profile. Thus, instead of accelerating as presented here, the vehicle could coast or continue to brake, depending on the situation. In some situations, such as switching into a faster lane of traffic, accelerating may be desirable.

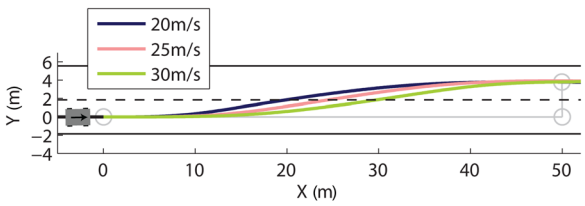

Fig. 13 Lane change paths traveled by vehicle

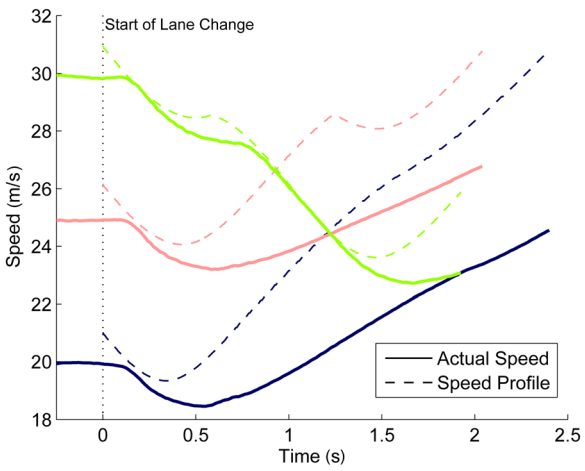

Fig. 14 Speed profile and actual vehicle speed

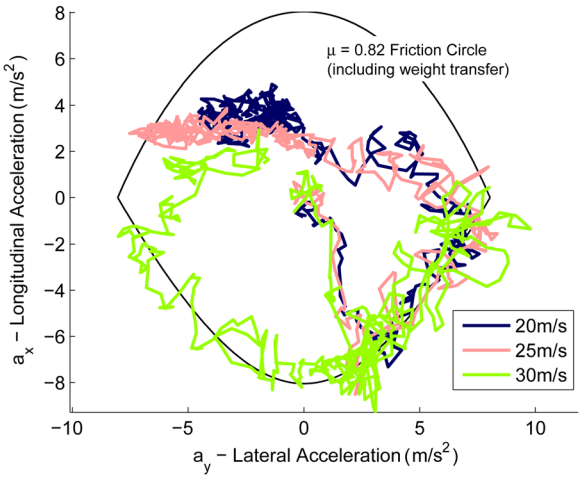

Fig. 15 Acceleration limits and experimental results

At 25 m/s, the vehicle calculated a path defined by $\gamma = 0.42$. The first elementary path still had larger curvature magnitude than the second, but the curvature difference was smaller than the 20 m/s case. If the vehicle could accelerate at the friction limits, it would need to brake during the second elementary path; however, because acceleration was limited by the engine, the vehicle never sped up enough to require braking. As a result, the vehicle braked at the beginning of the lane change and then accelerated through the remainder of the maneuver, similar to the 20 m/s case. The first elementary path of this lane change had lower curvature than that in the 20 m/s case, which resulted in vehicle accelerations at the friction limit for this higher speed.

When the obstacle was detected at 30 m/s, the path was calculated with $\gamma = 0.60$. Since $\gamma > 0.5$, the first elementary path had lower curvature magnitude than the second, shifting the vehicle into the new lane less rapidly than at the lower speeds. Lower curvature of the first elementary path allowed the vehicle to slow down while remaining within the friction limits, but the higher curvature of the second elementary path required lower speeds and further deceleration. As a result, the vehicle braked throughout the majority of the maneuver, as shown in Fig. 14. The resulting acceleration in Fig. 15 followed both sides of the negative a_x portion of the friction circle, corresponding to braking while turning both left and right. This path allowed the vehicle to combine steering and braking to not exceed the friction limits despite the higher initial speed; however, the path resulted in a speed profile with a significantly lower exit speed.

Stopping in the current lane could be an alternative to changing lanes in order to avoid an obstacle. While traveling at 20 m/s or 25 m/s, the vehicle could have stopped before the obstacle. At 30 m/s, assuming full braking at $a_x = -\mu g$, the vehicle would not have stopped in time and would have collided with the obstacle at over 9 m/s. Traveling at 30 m/s, changing lanes was necessary for collision avoidance.

6 Conclusion

Lane change trajectories can be constructed from bi-elementary paths and speed profiles. A candidate path's entry speed is a valid metric to judge path feasibility by ensuring it is lower than a vehicle's current speed. The approach presented here generates feasible lane change paths in real-time that can be driven up to modeled friction limits.

This analysis also suggests heuristics for bi-elementary lane change maneuvers. Steering while braking maximizes cases where

lane changes can be completed, and the relative amount of steering and braking changes with the longitudinal distance of the lane change. In all cases, faster steering allows higher speed lane changes.

Future work could analyze other lane change paths to determine whether bi-elementary path braking and steering heuristics extend to other path types and lane changes in general. The effects of transient vehicle dynamics could also be more fully explored to better quantify these limitations and their effect on a path's speed profile.

Acknowledgment

This research was supported by the Electronics Research Laboratory of Volkswagen of America (ERL). The authors would like to thank ERL employees Rob Simpson, Robert MacLellan, Larry Dirksen, and Pablo Marx, and Dynamic Design Lab colleagues Paul Theodosis, Nitin Kapania, and Rami Hindiyeh for their support of the project. Testing was made possible with the help of Thunderhill Raceway Park, especially with the assistance of David Vodden and Shannon Ell. Joseph Funke was supported by a Graduate Research Fellowship from the National Science Foundation.

References

[1] Dubins, L. E., 1957, "On Curves of Minimal Length With a Constraint on Average Curvature, and With Prescribed Initial and Terminal Positions and Tangents," Am. J. Math., **79**(3), pp. 497–516.

[2] Scheuer, A., and Fraichard, T., 1996, "Planning Continuous-Curvature Paths for Car-Like Robots," IEEE/RSJ International Conference on Intelligent Robots and Systems, Osaka, Japan, Nov. 4–8, pp. 1304–1311.

[3] Durali, M., Javid, G., and Kasaiezadeh, A., 2006, "Collision Avoidance Maneuver for an Autonomous Vehicle," 9th IEEE International Workshop on Advanced Motion Control, Istanbul, Turkey, pp. 249–254.

[4] Bianco, C. G. L., and Piazzi, A., 2000, "Optimal Trajectory Planning With Quintic G^2-Splines," Intelligent Vehicles Symposium, Dearborn, MI, pp. 620–625.

[5] Papadimitriou, I., and Tomizuka, M., 2003, "Fast Lane Changing Computations Using Polynomials," American Control Conference, Denver, CO, June 4–6, pp. 48–53.

[6] AASHTO, 2011, *A Policy on Geometric Design of Highways and Streets*, 6th ed., American Association of State Highway and Transportation Officials, Washington, DC.

[7] Kritayakirana, K., and Gerdes, J. C., 2012, "Autonomous Vehicle Control at the Limits of Handling," Int. J. Veh. Auton. Syst., **10**(4), pp. 271–296.

[8] Theodosis, P. A., and Gerdes, J. C., 2011, "Generating a Racing Line for an Autonomous Racecar Using Professional Driving Techniques," ASME Paper No. DSCC2011-6097.

[9] Urmson, C., Anhalt, J., Bagnell, D., Baker, C., Bittner, R., Clark, M. N., Dolan, J., Duggins, D., Gittleman, M., Harbaugh, S., Wolkowicki, Z., Ziglar, J., Bae, H., Brown, T., Demitrish, D., Sadekar, V., Zhang, W., Struble, J., Taylor, M., Darms, M., and Ferguson, D., 2008, "Autonomous Driving in Urban Environments: Boss and the Urban Challenge," J. Field Rob., **25**(8), pp. 425–466.

[10] Dolgov, D., Thrun, S., Montemerlo, M., and Diebel, J., 2010, "Path Planning for Autonomous Vehicles in Unknown Semi-Structured Environments," Int. J. Rob. Res., **29**(5), pp. 485–501.

[11] Werling, M., Kammel, S., Ziegler, J., and Groll, L., 2012, "Optimal Trajectories for Time-Critical Street Scenarios Using Discretized Terminal Manifolds," Int. J. Rob. Res., **31**(3), pp. 346–359.

[12] Xu, W., Wei, J., Dolan, J., Zhao, H., and Zha, H., 2012, "A Real-Time Motion Planner With Trajectory Optimization for Autonomous Vehicles," IEEE International Conference on Robotics and Automation, Saint Paul, MN, May 14–18, pp. 2061–2067.

[13] Hattori, Y., Ono, E., and Hosoe, S., 2008, "An Optimum Vehicle Trajectory Control for Obstacle Avoidance With the Shortest Longitudinal Traveling Distance," IEEE International Conference on Mechatronics and Automation, Takamatsu, Japan, Aug. 5–8, pp. 13–20.

[14] Kelly, D., and Sharp, R., 2010, "Time-Optimal Control of the Race Car: A Numerical Method to Emulate the Ideal Driver," Veh. Syst. Dyn., **48**(12), pp. 1461–1474.

[15] Nanao, M., and Ohtsuka, T., 2011, "Vehicle Dynamics Control for Collision Avoidance Considering Physical Limitations," IEEE Society of Instrumentation and Control Engineers Annual Conference, Tokyo, Japan, Sept. 13–18, pp. 688–693.

[16] Kanayama, Y. J., and Hartman, B. I., 1997, "Smooth Local-Path Planning for Autonomous Vehicles1," Int. J. Rob. Res., **16**(3), pp. 263–284.

[17] Kritayakirana, K., 2012, "Autonomous Vehicle Control at the Limits of Handling," Ph.D. thesis, Stanford University, Stanford, CA.

[18] Funke, J., Theodosis, P., Hindiyeh, R., Stanek, G., Kritatakirana, K., Gerdes, C., Langer, D., Hernandez, M., Muller-Bessler, B., and Huhnke, B., 2012, "Up to the Limits: Autonomous Audi TTS," IEEE Intelligent Vehicles Symposium (IV), Alcala de Henares, Spain, June 3–7, pp. 541–547.